gapless arcs that we observe are simply an intermediate state in the smooth evolution of *d*-wave nodes into a full Fermi surface. This smooth evolution was carefully checked on an 83 K underdoped sample where a detailed sweep was done in **k** space at $T = 90$ K, revealing only a small Fermi arc just above T_c. This behaviour is fully consistent with the gap above and below T_c being of the same origin as suggested by our earlier experiments[5,7].

Theoretical calculations in which *d*-wave pairing correlations cause a pseudogap above T_c (ref. 10) have predicted gapless arcs which expand as T increases. Resonating valence bond theories also lead to gapless arcs above T_c due to spinon pairing[11]. There are other proposals in which the pseudogap has a completely different (non-pairing) origin from the superconducting gap. Given the smooth evolution that we find through T_c, such proposals seem difficult to reconcile with our results. □

Received 23 July; accepted 22 December 1997.

1. Campuzano, J. C. *et al*. The Fermi surfaces of $YBa_2Cu_3O_{6.9}$ as seen by angle-resolved photoemission. *Phys. Rev. Lett.* **64,** 2308–2312 (1990).
2. Olson, C. G. *et al*. High-resolution angle-resolved photoemission study of the Fermi surface and normal-state electronic structure of $Bi_2Sr_2CaCu_2O_8$. *Phys. Rev. B* **42,** 381–386 (1990).
3. Randeria, M. *et al*. Momentum distribution sum rule for angle-resolved photoemission. *Phys. Rev. Lett.* **74,** 4951–4954 (1995).
4. Marshall, D. S. *et al*. Unconventional electronic structure evolution with hole doping in $Bi_2Sr_2CaCu_2O_{8+\delta}$: angle-resolved photoemission results. *Phys. Rev. Lett.* **76,** 4841–4844 (1996).
5. Ding, H. *et al*. Spectroscopic evidence for a pseudogap in the normal state of underdoped high-T_c superconductors. *Nature* **382,** 51–54 (1996).
6. Loeser, A. G. *et al*. Excitation gap in the normal state of underdoped $Bi_2Sr_2CaCu_2O_{8+\delta}$. *Science* **273,** 325–329 (1996).
7. Ding, H. *et al*. Evolution of the Fermi surface with carrier concentration in $Bi_2Sr_2CaCu_2O_{8+\delta}$. *Phys. Rev. Lett.* **78,** 2628–2631 (1997).
8. Uemura, Y. J. *et al*. Universal correlations between T_c and n_s/m^* in high-T_c cuprate superconductors. *Phys. Rev. Lett.* **62,** 2317–2320 (1989).
9. Lee, P. A. in *High Temperature Superconductivity* (eds Bedell, K. S. *et al.*) 96–116 (Addison-Wesley, New York, 1990).
10. Engelbrecht, J. R., Nazarenko, A., Randeria, M. & Dagotto, E. Pseudogap above T_c in a model with $d_{x^2-y^2}$ pairing. Preprint available at http://xxx.lanl.gov/archive/cond-mat/9705166
11. Wen, X. G. & Lee, P. A. Theory of underdoped cuprates. *Phys. Rev. Lett.* **76,** 503–506 (1996).
12. Ding, H. *et al*. Angle-resolved photoemission spectroscopy study of the superconducting gap anisotropy of $Bi_2Sr_2CaCu_2O_{8+x}$. *Phys. Rev. B* **54,** R9678–B9681 (1996).

Acknowledgements. We thank J. Sadleir and A. Kaminski for their help. This work was supported by the US Dept of Energy Basic Energy Sciences, the US NSF, the NSF Science and Technology Center for Superconductivity, the CREST of JST, and the Ministry of Education, Science and Culture of Japan. The Synchrotron Radiation Center is supported by the NSF.

Correspondence and requests for materials should be addressed to J.C.C. (e-mail: jcc@uic.edu).

A nanometre-scale mechanical electrometer

A. N. Cleland* & M. L. Roukes

Condensed Matter Physics 114-36, California Institute of Technology, Pasadena, California 91125, USA

The mechanical detection of charge has a long history, dating back more than 200 years to Coulomb's torsion-balance electrometer[1]. The modern analogues of such instruments are semiconductor-based field-effect devices, the most sensitive of which are cryogenically cooled single-electron transistors[2]. But although these latter devices have extremely high charge sensitivity, they suffer from limited bandwidth and must be operated at millikelvin temperatures in order to reduce thermal noise. Here we report the fabrication and characterization of a working nanometre-scale mechanical electrometer. We achieve a charge sensitivity of 0.1 e Hz$^{-0.5}$, competitive with conventional semiconductor field-effect transistors; moreover, thermal noise analysis indicates that the nanometre-scale electrometer should ultimately reach sensitivities of the order of 10^{-6} e Hz$^{-0.5}$, comparable with charge-detection capabilities of cryogenic single-electron transistors. The nanometre-scale electrometer has the additional advantages of high temperature (≥4.2 K) operation and response over a larger bandwidth, from which a diversity of applications may result.

We have described elsewhere[3] the techniques used to fabricate and measure devices of the type reported here. An electron micrograph and a schematic view of our nanomechanical electrometer is shown in Fig. 1. It consists of three principal components: electrodes, which experience an attractive force when a small charge is applied; a compliant mechanical element that moves in response to this force; and a displacement detector that provides a means of monitoring the motion. The mechanical element is a two-element torsional resonator with a spring constant G_0 and moment I. Its fundamental torsional resonance frequency is ω_0, and its mechanical loss is parametrized by a quality factor $Q = \omega_0/\Delta\omega$, where $\Delta\omega$ is the frequency width of the resonant response at half maximum.

The device includes three electrodes: two for inducing and measuring the mechanical response of the structure, and one for coupling charge, which alters this response. Two electrodes consist of metal loops tracing the boundaries of the outer and inner paddles, while the opposing metal gate electrode is fixed to the stationary substrate, at a distance d from the inner paddle. The mutual capacitance between the gate electrode and the inner paddle is represented by the parameter C. To measure a small charge, the gate electrode is biased by a charge q_0, which yields an electrostatic force $F_E = q_0^2/Cd$. Small changes in the coupled charge, δq, about the bias point q_0 alter the force by an amount $f_E = 2\delta q E_0$, where E_0 is the equilibrium electric field. This results in an effective torsional spring constant $G_{eff} = G_0 + g$, where $g = -r\partial q\partial E_0/\partial\theta$ (θ is the paddle torsion angle, E_θ the field component along the unit vector θ, and r the paddle's radial dimension). This gives rise to a shift away from the unperturbed resonance frequency, $\delta\omega/\omega_0 \approx g/2G_0$.

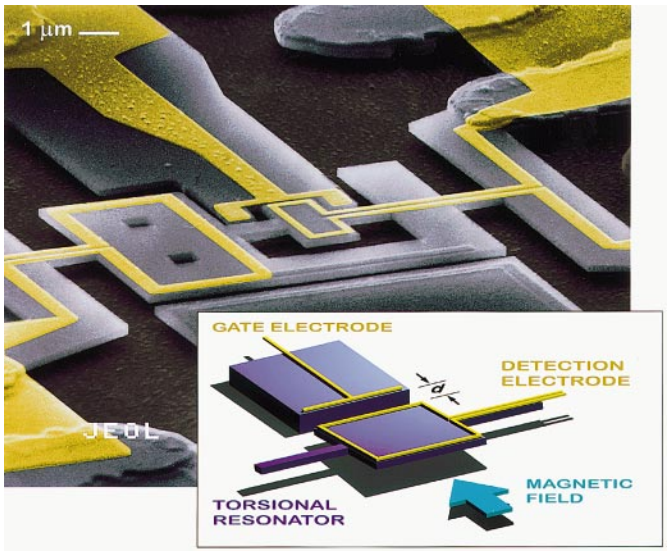

Figure 1 Nanometre-scale charge detector. The inset schematically depicts its principal components: torsional mechanical resonator, detection electrode, and gate electrode used to couple charge to the mechanical element. A external, parallel magnetic field is employed for readout. In the actual device (main figure) a double torsional element is used with moment I, torsional spring constant G_0 (calculated to be 1.1×10^{-10} N m), and spacing, $d = 0.5$ μm, between the gate and inner paddle electrodes. The fundamental resonance frequency of the structure is 2.61 MHz, with a quality factor measured to be $Q = 6{,}500$; the coupling capacitance between the gate and resonator was calculated to be $C = 0.4$ fF (H. Pothier, D. Esteve and M. H. Devoret, personal communication). The resonator was fabricated from a single-crystal Si-on-insulator substrate, with a 0.2-μm-thick Si layer on a 0.4-μm insulating layer. The Au electrodes and resonator structure are patterned using electron beam lithography. The smallest lateral feature in the structure is 0.2 μm, so there is scope to scale these devices to even smaller dimensions. This could ultimately yield bandwidths in the GHz regime.

* Present address: Department of Physics, UC Santa Barbara, Santa Barbara, California 93106, USA.

To perform electrometry we monitor either the charge-induced shift in the rest point of the torsional resonator, or the change in the resonance frequency due to the charge modulation of G_{eff}. The latter approach can be especially sensitive if the quality factor of the resonator is high. We have employed frequency modulation detection[4] to obtain enhanced sensitivity and large measurement bandwidth.

When optimally configured, thermally induced motion of the resonator limits the mechanical electrometer's sensitivity. Additional noise may be introduced by the displacement detector: with conventional optical detection this arises from photon shot noise, whereas with electromagnetic detection (used here) this arises from the readout amplifier. We parametrize this additional noise by a detection noise temperature T_N, while representing the thermal fluctuations of the mechanical resonator by a temperature T_R. For a paddle driven with a motional amplitude θ_{max}, the spectral density of the frequency noise is given as[5]:

$$S_\omega = \frac{\omega_0 k_B (T_R + T_N)}{Q G_0 \theta_{max}^2} \quad (1)$$

The corresponding charge noise spectral density is given by:

$$S_q = \frac{G_0}{\partial E_0/\partial\theta}\frac{1}{\omega_0^2 S_\omega} \quad (2)$$

In our experiments we use these devices for charge detection by employing the fundamental torsional mode (both elements of the torsional structure vibrate with similar amplitude and phase). The resonator was placed in vacuum at 4.2 K. A radio frequency (r.f.) current was passed through the larger gold loop which, in the presence of an applied 8 T magnetic field, generates a r.f. torque along the support axis of the resonator. The resulting torsional motion of the resonator's inner paddle in the applied field generates an electromotive force (EMF) that is subsequently amplified and detected by room-temperature electronics. Related techniques have been used to detect the motion of flexural resonators[6,7].

In Fig. 2 we show the amplitude of the EMF measured as a function of drive current frequency, with fixed current amplitude. Each trace was taken with a different amount of d.c. voltage applied to the gate electrode. The range of voltages applied corresponds to a total change in the coupled charge of $\sim 4 \times 10^4\, e$.

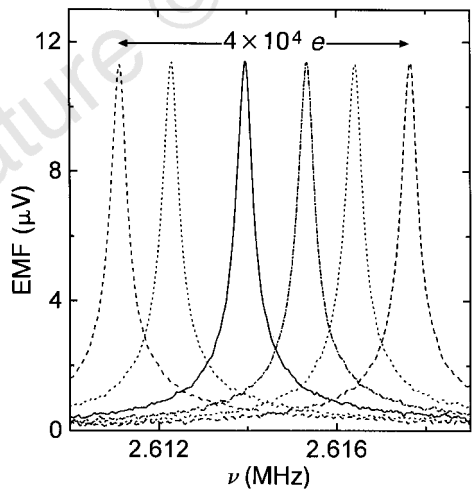

Figure 2 Amplitude of the induced EMF across the small loop (inner paddle) of the resonator, as a function of the frequency of the drive current passed through the large loop (outer paddle). The charge coupled by the gate electrode was changed in steps for each trace, with a total range of $4 \times 10^4\, e$ in the coupled charge. The charge sensitivity is referenced to the charge coupled directly to the resonator paddle; we ignore the large amount of charge induced by our voltage bias on the parasitic capacitances associated with the cabling. In real charge-detection applications of this device, the charge source would necessarily be placed, at most, a few tens of micrometres from the gate. This constraint is identical to those arising in applications based on the single-electron transistor, and is not a serious limitation.

A more sensitive detection technique is to fix the frequency of the drive current at the mechanical resonance frequency, and monitor the phase of the induced EMF relative to the phase of the drive current. The circuit used for this measurement is shown in Fig. 3. In the inset of Fig. 4 we show the frequency-dependent phase responsibility $R = \partial\phi/\partial q(\nu)$, which is the measured variation of the EMF phase as a function of d.c. coupled charge. By measuring the spectral density of the phase noise, $S_\phi(\nu)$, we can then deduce the spectral density of the charge noise $S_Q(\nu) = S_\phi(\nu)/R^2$ (Fig. 4). We find the charge noise to be dominated by $1/f$ noise at low frequencies, with a noise level of $S_Q^{0.5} = 0.6\, e\,\mathrm{Hz}^{-0.5}$ at $\nu = 10$ Hz. Above a frequency of about 500 Hz the noise levels out to a white noise floor of $S_Q^{0.5} = 0.09\, e\,\mathrm{Hz}^{-0.5}$. The lowest level of charge noise obtained is $\sim 0.1\, e\,\mathrm{Hz}^{-0.5}$, competitive with state-of-the-art electrometers based on cryogenically cooled field-effect transistors[8].

Mechanical detection of charge has been previously demonstrated[9,10] using an atomic force microscope (AFM) apparently providing sensitivity as low as $0.03\, e\,\mathrm{Hz}^{-0.5}$. This was achieved using cantilevers with $\sim 100\,\mu$m dimensions and resonance frequencies in the audio range. Their intrinsically low response frequency and the overall size of these macroscopic AFM instruments makes them impractical for general applications in electrometry. Nonetheless, one may consider our devices to be an extension of the principles demonstrated by such AFM charge detection—but carried to much smaller geometries, higher resonance frequencies, and achieved within an entirely integrated, nanomachined structure.

These nanometre-scale mechanical electrometers show that greatly enhanced sensitivity can be expected with future improvements to device design. Our measurements indicate that the $1/f$ noise in these devices emanates from the resonator or the charge coupled to it, similar to findings with the single electron transistor[2]. This should be susceptible to careful surface passivation. The measurement bandwidth can be increased using feedback techniques[4], with which we achieved a bandwidth of 10 kHz and a noise of $2\, e\,\mathrm{Hz}^{-0.5}$, limited by the room-temperature feedback amplifier. Use of a cryogenic amplifier would lead to significantly improved sensitivity.

We now consider the ultimate theoretical limits to the performance of these devices. The charge noise floor is set by the precision of the measurement of resonance frequency. This, in turn, is limited

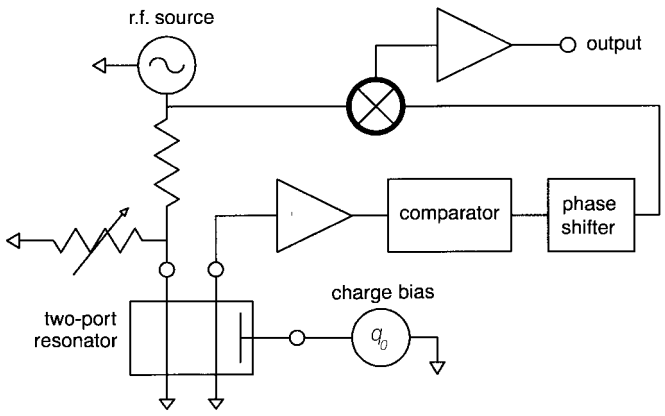

Figure 3 Measurement scheme used to measure changes in the phase of the induced EMF as a function of coupled charge, for fixed drive current frequency of 2.617 MHz. The bandwidth obtained with this technique is limited to $\nu_0/Q = 400$ Hz, due to uncontrolled parasitic capacitances in these prototype devices.

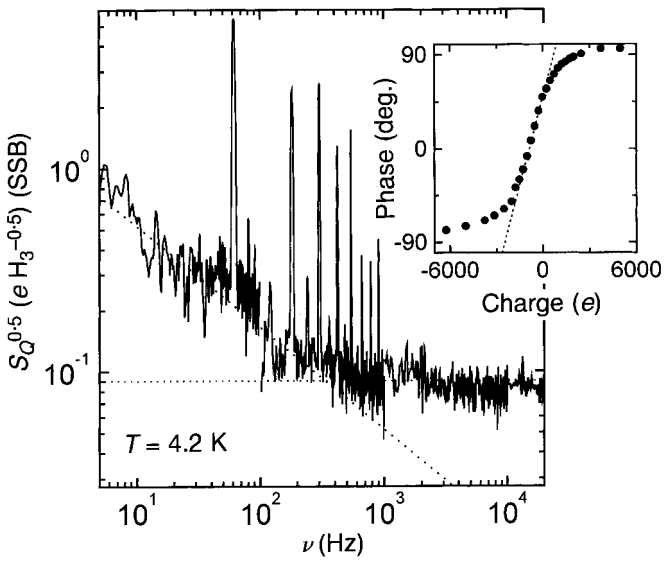

Figure 4 Measured charge noise as a function of frequency, using the measurement set-up shown in Fig. 3. The noise, measured at the output of a mixer, is scaled to single-sideband value. The horizontal dotted line is the white noise level of 0.09 e $Hz^{-0.5}$, and the sloped dotted line is the level of 1/f noise. Inset, measured phase variation as a function of d.c. coupled charge to the gate. The dotted line indicates the zero-frequency charge responsivity. Measurement performed using set-up in Fig. 3.

by thermal noise in the resonator and the readout amplifier, as given by equation (1). For enhanced sensitivity, we need low noise temperatures, high quality factors, Q, and large drive amplitudes, θ (limited, however, by the onset of nonlinearity at large θ.) Large-radii paddles with small electrode spacing are advantageous, but the accompanying increase in the paddle inertia I, and reduction in frequency ν_0, is deleterious, so careful optimization is required.

For our device design we can estimate the thermal limit to the charge sensitivity. With a drive amplitude of 30 mrad and a readout amplifier noise temperature of 300 K (roughly the value in the experiment), a voltage bias of 10 V on the gate gives a thermally limited charge noise of $7 \times 10^{-4}\, e\,\mathrm{Hz}^{-0.5}$. A state-of-the-art cryogenic amplifier (noise temperature $\sim$ 10 K) reduces this to $1 \times 10^{-4}\, e\,\mathrm{Hz}^{-0.5}$. This becomes comparable to a single-electron transistor operating at 50 mK and measured at 1 kHz, where it is limited by 1/f process[2,11]. If we reduce the torsional rod cross-section while increasing its length, so that each rod has dimensions $0.1 \times 0.1 \times 2\,\mu\mathrm{m}^3$, and the paddle dimensions are reduced to $0.1 \times 0.5 \times 1\,\mu\mathrm{m}^3$ (here the last dimension is the paddle radius, r), we obtain a resonance frequency $\nu_0 = 7$ MHz. Placing the gate electrode 0.1 μm from the paddle edge, we obtain a charge noise floor of $\sim 3 \times 10^{-6}\, e\,\mathrm{Hz}^{-0.5}$, an improvement of nearly two orders of magnitude.

These experimental prototypes clearly show that nanometre-scale mechanical electrometry provides a new means for ultrasensitive charge measurement; they are unique in that they offer a much higher potential bandwidth than the single-electron transistor. A further advantage is their ability to operate at 4.2 K (or higher), as compared to the millikelvin temperatures required for very low noise single-electron transistors. This opens possibilities for applications such as single-photon photodetection[12] or ultrasensitive scanned electrometry[13]. □

Received 14 August; accepted 29 December 1997.

1. Coulomb, C. A. *Memoires de l'Academie Royale des Sciences* 229–236 (Academie royale des sciences, Paris, 1784).
2. Zimmerli, G., Eiles, T. M., Kautz, R. L. & Martinis, J. M. Noise in the Coulomb blockade electrometer. *Appl. Phys. Lett.* **61,** 237–239 (1992).
3. Cleland, A. N. & Roukes, M. L. Fabrication of high frequency nanometer scale mechanical resonators from bulk Si crystals. *Appl. Phys. Lett.* **69,** 2653–2655 (1996).
4. Albrecht, T. R., Grutter, P., Horne, D. & Rugar, D. Frequency modulation detection using high-Q cantilevers for enhanced force microscope sensitivity. *J. Appl. Phys.* **69,** 668–673 (1991).
5. Robins, W. P. *Phase Noise in Signal Sources: Theory and Applications* (Peregrinus, London, 1984).
6. Greywall, D. S., Yurke, B., Busch, P. A., Pargellis, A. N. & Willett, R. L. Evading amplifier noise in nonlinear oscillators. *Phys. Rev. Lett.* **72,** 2992–2995 (1994).
7. Yurke, B., Greywall, D. S., Pargellis, A. N. & Busch, P. A. Theory of amplifier noise evasion in an oscillator employing a nonlinear resonator. *Phys. Rev. A* **51,** 4211–4229 (1995).
8. Bordoni, F., Maggi, G., Ottaviano, A. & Pallotino, G. V. Very low noise cooled audiofrequency preamplifier for gravitational research. *Rev. Sci. Instrum.* **52,** 1079–1086 (1981).
9. Stern, J. E., Terris, B. D., Mamin, H. J. & Rugar, D. Deposition and imaging of localized charge in insulator surfaces using a force microscope. *Appl. Phys. Lett.* **53,** 2717–2719 (1988).
10. Schonenberger, C. & Alvarado, S. F. Observation of single charge carriers by force microscopy. *Phys. Rev. Lett.* **65,** 3162–3164 (1990).
11. Pendry, J. B., Kirkman, P. D. & Castano, E. Electrons at disordered surfaces and 1/f noise. *Phys. Rev. Lett.* **57,** 2983–2986 (1986).
12. Cleland, A. N., Esteve, D., Urbina, C. & Devoret, M. H. Very low noise photodector based on the single electron transistor. *Appl. Phys. Lett.* **61,** 2820–2822 (1992).
13. Yoo, M. J. *et al.* Scanning single-electron transistor microscopy: Imaging individual charges. *Science* **276,** 579–582 (1997).

Acknowledgements. This work was supported by DARPA ETO/MEMS.

Correspondence and requests for materials should be addressed to M.L.R. (e-mail: roukes@caltech.edu).

Discovery of a useful thin-film dielectric using a composition-spread approach

R. B. van Dover, L. F. Schneemeyer & R. M. Fleming

Bell Laboratories, Lucent Technologies, Murray Hill, New Jersey 07974, USA

The continuing drive towards miniaturization of electronic devices[1] is motivating the search for new materials. Consider, for example, the case of the much-used dynamic random-access memory. The minimum capacitance per cell that can be tolerated is expected[2] to remain at 30–40 fF, but as the cell area decreases, the corresponding reduction in geometric capacitance has to be compensated for. So far, this has been achieved by resorting to complex non-planar structures and/or using much thinner films of the dielectric insulator, amorphous silicon dioxide (a-SiO_x), although the latter approach is limited by the electric fields that can be supported by a-SiO_x before its insulating properties break down. An alternative strategy is to develop thin-film insulators that have a dielectric constant significantly greater than that of a-SiO_x, reducing the size of the fields required for device operation. Here we show that a composition-spread technique allows for the efficient evaluating of materials with both a high dielectric constant and a high breakdown field. We apply this approach to the Zr–Sn–Ti–O system, and we find that compositions close to $Zr_{0.15}Sn_{0.3}Ti_{0.55}O_{2-\delta}$ are better thin-film dielectrics than high-quality deposited a-SiO_x. Although detailed tests of the performance of these materials have not yet been carried out, our initial results suggest that they are likely to be comparable to the best alternatives (such as (Ba, Sr)TiO_3) currently being considered for integrated-circuit capacitors.

Initial assessment of a new material demands the choice of a suitable criterion that can distinguish promising materials from those with little potential. For capacitor materials, the key parameters are the capacitance per unit area (C/A) and maximum working voltage (V_{br}). A useful figure of merit[3] (FOM) can be defined as the product of these, that is, FOM = CV_{br}/A. As $C = \epsilon_r\epsilon_0 A/d$ and $V_{br} = E_{br}d$, where d is the dielectric thickness, ϵ_r the dielectric constant, ϵ_0 the permittivity of free space, and E_{br} the breakdown field, FOM can also be defined as FOM = $\epsilon_r\epsilon_0 E_{br}$. Defined in this way, FOM corresponds to the maximum charge that can be stored on a capacitor made from a given material. It is independent of film thickness to the degree that ϵ_r and E_{br} are. Note that the useful working voltage may be much less than the maximum working